Measurements of J/ψ decays into $\omega\pi^0$, $\omega\eta$, and $\omega\eta'$

M. Ablikim[1], J. Z. Bai[1], Y. Ban[11], J. G. Bian[1], X. Cai[1], H. F. Chen[16], H. S. Chen[1], H. X. Chen[1], J. C. Chen[1], Jin Chen[1], Y. B. Chen[1], S. P. Chi[2], Y. P. Chu[1], X. Z. Cui[1], Y. S. Dai[18], Z. Y. Deng[1], L. Y. Dong[1a], Q. F. Dong[14], S. X. Du[1], Z. Z. Du[1], J. Fang[1], S. S. Fang[2], C. D. Fu[1], C. S. Gao[1], Y. N. Gao[14], S. D. Gu[1], Y. T. Gu[4], Y. N. Guo[1], Y. Q. Guo[1], Z. J. Guo[15], F. A. Harris[15], K. L. He[1], M. He[12], Y. K. Heng[1], H. M. Hu[1], T. Hu[1], G. S. Huang[1b], X. P. Huang[1], X. T. Huang[12], X. B. Ji[1], X. S. Jiang[1], J. B. Jiao[12], D. P. Jin[1], S. Jin[1], Yi Jin[1], Y. F. Lai[1], G. Li[2], H. B. Li[1], H. H. Li[1], J. Li[1], R. Y. Li[1], S. M. Li[1], W. D. Li[1], W. G. Li[1], X. L. Li[8], X. Q. Li[10], Y. L. Li[4], Y. F. Liang[13], H. B. Liao[6], C. X. Liu[1], F. Liu[6], Fang Liu[16], H. H. Liu[1], H. M. Liu[1], J. Liu[11], J. B. Liu[1], J. P. Liu[17], R. G. Liu[1], Z. A. Liu[1], F. Lu[1], G. R. Lu[5], H. J. Lu[16], J. G. Lu[1], C. L. Luo[9], F. C. Ma[8], H. L. Ma[1], L. L. Ma[1], Q. M. Ma[1], X. B. Ma[5], Z. P. Mao[1], X. H. Mo[1], J. Nie[1], S. L. Olsen[15], H. P. Peng[16], N. D. Qi[1], H. Qin[9], J. F. Qiu[1], Z. Y. Ren[1], G. Rong[1], L. Y. Shan[1], L. Shang[1], D. L. Shen[1], X. Y. Shen[1], H. Y. Sheng[1], F. Shi[1], X. Shi[11c], H. S. Sun[1], J. F. Sun[1], S. S. Sun[1], Y. Z. Sun[1], Z. J. Sun[1], Z. Q. Tan[4], X. Tang[1], Y. R. Tian[14], G. L. Tong[1], G. S. Varner[15], D. Y. Wang[1], L. Wang[1], L. S. Wang[1], M. Wang[1], P. Wang[1], P. L. Wang[1], W. F. Wang[1d], Y. F. Wang[1], Z. Wang[1], Z. Y. Wang[1], Zhe Wang[1], Zheng Wang[2], C. L. Wei[1], D. H. Wei[1], N. Wu[1], X. M. Xia[1], X. X. Xie[1], B. Xin[8b], G. F. Xu[1], Y. Xu[10], M. L. Yan[16], F. Yang[10], H. X. Yang[1], J. Yang[16], Y. X. Yang[3], M. H. Ye[2], Y. X. Ye[16], Z. Y. Yi[1], G. W. Yu[1], C. Z. Yuan[1], J. M. Yuan[1], Y. Yuan[1], S. L. Zang[1], Y. Zeng[7], Yu Zeng[1], B. X. Zhang[1], B. Y. Zhang[1], C. C. Zhang[1], D. H. Zhang[1], H. Y. Zhang[1], J. W. Zhang[1], J. Y. Zhang[1], Q. J. Zhang[1], X. M. Zhang[1], X. Y. Zhang[12], Yiyun Zhang[13], Z. P. Zhang[16], Z. Q. Zhang[5], D. X. Zhao[1], J. W. Zhao[1], M. G. Zhao[10], P. P. Zhao[1], W. R. Zhao[1], Z. G. Zhao[1e], H. Q. Zheng[11], J. P. Zheng[1], Z. P. Zheng[1], L. Zhou[1], N. F. Zhou[1], K. J. Zhu[1], Q. M. Zhu[1], Y. C. Zhu[1], Y. S. Zhu[1], Yingchun Zhu[1f], Z. A. Zhu[1], B. A. Zhuang[1], X. A. Zhuang[1], B. S. Zou[1]
(BES Collaboration)

[1] Institute of High Energy Physics, Beijing 100049, People's Republic of China
[2] China Center for Advanced Science and Technology(CCAST), Beijing 100080, People's Republic of China
[3] Guangxi Normal University, Guilin 541004, People's Republic of China
[4] Guangxi University, Nanning 530004, People's Republic of China
[5] Henan Normal University, Xinxiang 453002, People's Republic of China
[6] Huazhong Normal University, Wuhan 430079, People's Republic of China
[7] Hunan University, Changsha 410082, People's Republic of China
[8] Liaoning University, Shenyang 110036, People's Republic of China
[9] Nanjing Normal University, Nanjing 210097, People's Republic of China
[10] Nankai University, Tianjin 300071, People's Republic of China
[11] Peking University, Beijing 100871, People's Republic of China
[12] Shandong University, Jinan 250100, People's Republic of China
[13] Sichuan University, Chengdu 610064, People's Republic of China
[14] Tsinghua University, Beijing 100084, People's Republic of China
[15] University of Hawaii, Honolulu, HI 96822, USA
[16] University of Science and Technology of China, Hefei 230026, People's Republic of China
[17] Wuhan University, Wuhan 430072, People's Republic of China
[18] Zhejiang University, Hangzhou 310028, People's Republic of China

[a] Current address: Iowa State University, Ames, IA 50011-3160, USA
[b] Current address: Purdue University, West Lafayette, IN 47907, USA
[c] Current address: Cornell University, Ithaca, NY 14853, USA
[d] Current address: Laboratoire de l'Accélérateur Linéaire, Orsay, F-91898, France
[e] Current address: University of Michigan, Ann Arbor, MI 48109, USA
[f] Current address: DESY, D-22607, Hamburg, Germany

Based on $5.8 \times 10^7 J/\psi$ events collected with BESII at the Beijing Electron-Positron Collider (BEPC), the decay branching fractions of $J/\psi \to \omega\pi^0$, $\omega\eta$, and $\omega\eta'$ are measured using different η and η' decay modes. The results are higher than previous measurements. The $\omega\pi^0$ electromagnetic form factor is also obtained.

PACS numbers: 13.25.Gv, 12.38.Qk, 14.40.Gx

I. INTRODUCTION

The decay of the J/ψ into a vector and pseudoscalar (VP) meson pair proceeds via $c\bar{c}$ annihilation to three gluons in strong decays and to one virtual photon in electromagnetic decays. A full set of $J/\psi \to VP$ measurements allows one to systematically study the quark-gluon content of pseudoscalar mesons and SU(3) breaking, as well as determine the contribution of different amplitudes to the decay rates in two-body J/ψ decays [1]. Measurements of purely electromagnetic J/ψ decays can be used to calculate the electromagnetic form factors involved; those form factors are used to test QCD inspired models of the mesonic wave function. MARKIII [2, 3] and DM2 [4] measured many $J/\psi \to VP$ branching fractions and obtained the $\eta - \eta'$ mixing angle, the quark content of the η and η', and much more.

Recently, a sample of $5.8 \times 10^7 J/\psi$ events, which offers a unique opportunity to measure the full set of $J/\psi \to VP$ decays precisely, was accumulated with the upgraded Beijing Spectrometer (BESII) [5]. In an earlier analysis based on this data set and using a GEANT3 based Monte-Carlo with a careful simulation of detector response, the branching fraction of $J/\psi \to \pi^+\pi^-\pi^0$ was measured to be (2.10±0.12)% [6], which is higher than the PDG [7] value by about 30%. This indicates a higher branching fraction for $J/\psi \to \rho\pi$ than those from older experiments [7]. Furthermore, the branching ratios of $J/\psi \to \phi P(\pi^0, \eta, \eta')$ [8] are also higher than old experimental results. Therefore, remeasuring the branching fractions of all $J/\psi \to VP$ decay modes becomes very important. In this paper, $J/\psi \to \omega\pi^0$, $\omega\eta$, and $\omega\eta'$ are studied using different η and η' decay modes.

II. THE BES DETECTOR

The upgraded Beijing Spectrometer detector (BESII) is located at the Beijing Electron-Positron Collider (BEPC). BESII is a large solid-angle magnetic spectrometer which is described in detail in Ref. [5]. The momentum of charged particles is determined by a 40-layer cylindrical main drift chamber (MDC) which has a momentum resolution of σ_p/p=1.78%$\sqrt{1+p^2}$ (p in GeV/c). Particle identification is accomplished using specific ionization (dE/dx) measurements in the drift chamber and time-of-flight (TOF) information in a barrel-like array of 48 scintillation counters. The dE/dx resolution is $\sigma_{dE/dx} \simeq 8.0\%$; the TOF resolution for Bhabha events is $\sigma_{TOF} = 180$ ps. Radially outside of the time-of-flight counters is a 12-radiation-length barrel shower counter (BSC) comprised of gas tubes interleaved with lead sheets. The BSC measures the energy and direction of photons with resolutions of $\sigma_E/E \simeq 21\%\sqrt{E}$ (E in GeV), $\sigma_\phi = 7.9$ mrad, and $\sigma_z = 2.3$ cm. The iron flux return of the magnet is instrumented with three double layers of proportional counters that are used to identify muons.

A GEANT3 based Monte Carlo (MC) package (SIMBES) [9] with detailed consideration of the detector performance is used. The consistency between data and MC has been carefully checked in many high purity physics channels, and the agreement is reasonable. More details on this comparison can be found in Ref. [9]. In this analysis, the detection efficiency and mass resolution for each decay mode are obtained from a MC simulation, which takes into account the angular distributions appropriate for the different final states [10].

III. ANALYSIS

In this analysis, the ω meson is observed in its $\pi^+\pi^-\pi^0$ decay mode, and the pseudoscalar mesons are detected in the modes: $\pi^0 \to \gamma\gamma$; $\eta \to \gamma\gamma$, $\gamma\pi^+\pi^-$, and $\pi^+\pi^-\pi^0$; and $\eta' \to \gamma\pi^+\pi^-(\gamma\rho)$ and $\pi^+\pi^-\eta$ ($\eta \to \gamma\gamma$). Using the different η and η' decay modes allows us to cross check our measurements, as well as obtain higher precision. Possible final states of $J/\psi \to \omega\pi^0$, $\omega\eta$, and $\omega\eta'$ are then $\pi^+\pi^-\gamma\gamma\gamma\gamma$, $\pi^+\pi^-\pi^+\pi^-\gamma\gamma\gamma$, and $\pi^+\pi^-\pi^+\pi^-\gamma\gamma\gamma\gamma$.

Candidate events are required to satisfy the following common selection criteria:

1. Events must have two or four good charged tracks with zero net charge. A good charged track is a track that is well fitted to a helix, originates from the interaction region of R_{xy} <0.02 m and $|z| < 0.2$ m, and has a polar angle, θ, in

the range $|\cos\theta| < 0.8$. R_{xy} is the distance from the beamline to the point of closest approach of the track to the beamline, and $|z|$ is the distance along the beamline to this point from the interaction point.

2. Candidate events should have at least the minimum number of isolated photons associated with the different final states, unless otherwise specified. Isolated photons are those that have energy deposited in the BSC greater than 60 MeV, the angle between the photon entering the BSC and the shower development direction in the BSC less than 30°, and the angle between the photon and any charged track larger than 10°.

3. For each charged track in an event, $\chi^2_{PID}(i)$ is determined using both dE/dx and TOF information:

$$\chi^2_{PID}(i)=\chi^2_{dE/dx}(i)+\chi^2_{TOF}(i),$$

where i corresponds to the particle hypothesis. A charged track is identified as a π if χ^2_{PID} for the π hypothesis is less than those for the K or p hypotheses. For the channels studied, at least one charged track must be identified as a pion.

4. The selected events are subjected to four constraint (4-C) kinematic fits, unless otherwise specified. When there are more than the minimum number of photons in an event, all combinations are tried, and the combination with the smallest χ^2 is retained. The χ^2 values required in the selection of events below are based on the optimization of $S/\sqrt{S+B}$, where the S and B are the expected signal and background, respectively.

The branching fraction is calculated using

$$B(J/\psi \to \omega P) = \frac{N_{obs}}{N_{J/\psi} \cdot \varepsilon \cdot B(\omega \to \pi^+\pi^-\pi^0) \cdot B(P \to X) \cdot B(\pi^0 \to \gamma\gamma)}$$

where N_{obs} is the number of events observed, $N_{J/\psi}$ is the total number of J/ψ events, $(5.77\pm0.27)\times10^7$ [11], ε is the detection efficiency obtained from MC simulation which takes into account the angular distributions [10], and $B(\omega \to \pi^+\pi^-\pi^0)$ and $B(P \to X)$ are the branching fractions, taken from the Particle Data Group (PDG) [7], of $\omega \to \pi^+\pi^-\pi^0$ and the pseudoscalar P to X final states, respectively.

A. $J/\psi \to \omega\gamma\gamma$

Events with two oppositely charged tracks and at least four isolated photons are selected. A 4C-fit is performed to the $\pi^+\pi^-\gamma\gamma\gamma\gamma$ hypothesis, and $\chi^2 < 15$ is required. There are six $\gamma\gamma$ combinations to test for consistency with the π^0 mass. Looping over all combinations, we calculate $m_{\pi^+\pi^-\gamma_1\gamma_2}$ for combinations satisfying $|m_{\gamma_1\gamma_2} - 0.135| < 0.04$ GeV/c^2, denoted as $m_{\pi^+\pi^-\pi^0}$, and plot $m_{\pi^+\pi^-\pi^0}$ versus $m_{\gamma_3\gamma_4}$ in Fig. 1, where clear π^0 and η signals are seen.

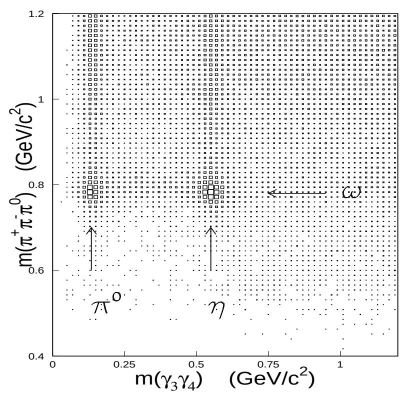

FIG. 1: Scatter plot of $m_{\gamma_3\gamma_4}$ versus $m_{\pi^+\pi^-\pi^0}$ for $J/\psi \to \pi^+\pi^-\gamma\gamma\gamma\gamma$ candidate events.

1. $J/\psi \to \omega\pi^0$

The $m_{\pi^+\pi^-\pi^0}$ distribution for events with the recoil $\gamma\gamma$ invariant mass ($\gamma_3\gamma_4$) being in the π^0 mass region, $|m_{\gamma_3\gamma_4} - 0.135| < 0.04$ GeV/c^2, is shown as crosses in Fig. 2. The ω signal, clearly seen in Fig. 2, is fitted to obtain the branching fraction of $J/\psi \to \omega\pi^0$. Backgrounds for $J/\psi \to \omega\pi^0$ which contribute to the peak in the ω signal region mainly come from non-π^0 events and events from $J/\psi \to \omega\eta(\eta \to \pi^0\pi^0\pi^0)$ and $\omega\pi^0\pi^0$ that survive selection criteria. Non-π^0 events can be measured using π^0 sideband events ($0.25 < m_{\gamma_3\gamma_4} <$ 0.40 GeV/c^2). These backgrounds will be subtracted after the fit.

A fit to the $m_{\pi^+\pi^-\pi^0}$ distribution is performed using the expected ω shape obtained from MC simulation and a first order polynomial background, shown as the curve in Fig. 2, and 2595 ± 59 ω events are obtained. The inset in Fig. 2 shows the fit with a second order polynomial background. The $m_{\pi^+\pi^-\pi^0}$ distribution for events which recoil against the π^0 sideband region ($0.25 < m_{\gamma_3\gamma_4} < 0.40$ GeV/c^2), shown in Fig. 3, is fitted to determine the non-π^0 background; after

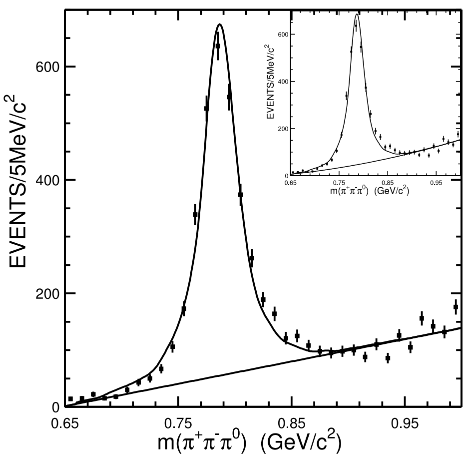

FIG. 2: The $m_{\pi^+\pi^-\pi^0}$ invariant mass distribution for $J/\psi \to \omega\pi^0$ candidate events. The curves are the results of the fit described in the text. The inset is the fit using a different background shape (second order polynomial).

normalization, 242 ± 10 non-ω background events are obtained and subtracted. We also subtract 142 ± 18 background events from $J/\psi \to \omega\eta(\eta \to \pi^0\pi^0\pi^0)$ and 121 ± 25 from $J/\psi \to \omega\pi^0\pi^0$, which are estimated from Monte Carlo simulation.

Since $J/\psi \to \omega\pi^0$ is an isospin violation process, the continuum contribution might be sizable in this channel, while it can be neglected in $J/\psi \to \omega\eta$ and $\omega\eta'$ decays. To determine background contamination from continuum production, the $L = 2347.3$ nb^{-1} data sample taken at $\sqrt{s} = 3.07$ GeV is analyzed using the same event selection, and after normalization 53 ± 22 continuum background events are estimated. The continuum contribution is subtracted without considering possible interference. Backgrounds from other channels are negligible. The detection efficiency for the signal is 7.55%, which is determined by MC simulation, and the branching ratio for this channel is

$$B(J/\psi \to \omega\pi^0) = (5.38 \pm 0.12) \times 10^{-4}.$$

Here, the error is statistical only.

This decay is an isospin-violating, electromagnetic process, and we calculate the electromagnetic form factor using the above branching ratio, according to the formula

$$\frac{|f(m^2_{J/\psi})|^2}{|f(0)|^2} = \frac{\alpha}{3} \cdot [\frac{p_\gamma}{p_\omega}]^3 \cdot \frac{m_{J/\psi}\Gamma(J/\psi \to \omega\pi^0)}{\Gamma(J/\psi \to \gamma\pi^0) \cdot \Gamma(J/\psi \to \mu^+\mu^-)}.$$

It gives $|f(m^2_{J/\psi})|/|f(0)| = 0.0411 \pm 0.0009$, which is consistent with that of MarkIII [3] but is three times smaller than that of $J/\psi \to p\bar{p}$ [12].

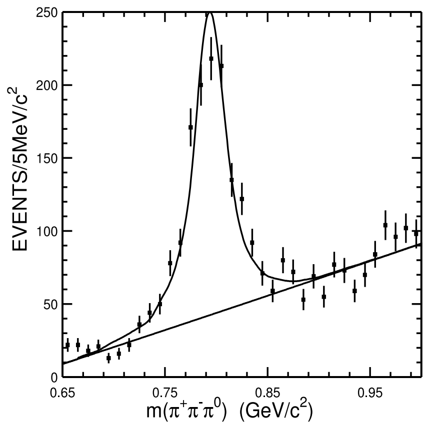

FIG. 3: The $m_{\pi^+\pi^-\pi^0}$ distribution for events recoiling against the π^0 sideband region ($0.25 < m_{\gamma_3\gamma_4} < 0.40$ GeV/c^2).

2. $J/\psi \to \omega\eta$

The $m_{\pi^+\pi^-\pi^0}$ distribution for events where the $\gamma\gamma$ invariant mass is required to be in the η mass region, $|m_{\gamma_3\gamma_4} - 0.547| < 0.04$ GeV/c^2, is shown in Fig. 4. A clear ω signal can be seen. The main background events for $J/\psi \to \omega\eta$ come from non-η events and the events from $J/\psi \to \omega\eta$, $\eta \to \pi^0\pi^0\pi^0$ and $J/\psi \to \omega\pi^0\pi^0$. Fitting the $m_{\pi^+\pi^-\pi^0}$ distribution in Fig. 4 with the ω shape from Monte Carlo simulation plus a first order polynomial background gives 3790 ± 72 candidate ω events. Using the same procedure to fit the $m_{\pi^+\pi^-\pi^0}$ distribution recoiling against the η sideband ($0.65 < m_{\gamma\gamma} < 0.80$ GeV/c^2) and normalizing, 188 ± 18 non-η background events are estimated. We also subtract the 161 ± 17 and 30 ± 4 background events from $J/\psi \to \omega\eta$, $\eta \to \pi^0\pi^0\pi^0$ and $J/\psi \to \omega\pi^0\pi^0$, respectively, which are estimated by MC simulation. The detection efficiency for $J/\psi \to \omega\eta$, $\eta \to \gamma\gamma$ determined from MC simulation is 7.45%; thus the $J/\psi \to \omega\eta$ branching fraction is

$$B(J/\psi \to \omega\eta) = (22.86 \pm 0.43) \times 10^{-4},$$

where the error is statistical only.

Fig. 5 shows the χ^2 distributions for the 4C fits to the $J/\psi \to \pi^+\pi^-\gamma\gamma\gamma\gamma$ hypothesis for $J/\psi \to \omega\eta$ candidate events ($|m_{\gamma_3\gamma_4} - 0.547| < 0.04$ GeV/c^2 and $|m_{\pi^+\pi^-\pi^0} - 0.782| < 0.04$ GeV/c^2), where the crosses are data and the histogram is the sum of MC simulation of the signal channel $J/\psi \to \omega\eta$ and the backgrounds from non-η events, measured using η sidebands, as well as from $J/\psi \to \omega\eta(\eta \to \pi^0\pi^0\pi^0)$ and $J/\psi \to \omega\pi^0\pi^0$. They agree with each other reasonably well.

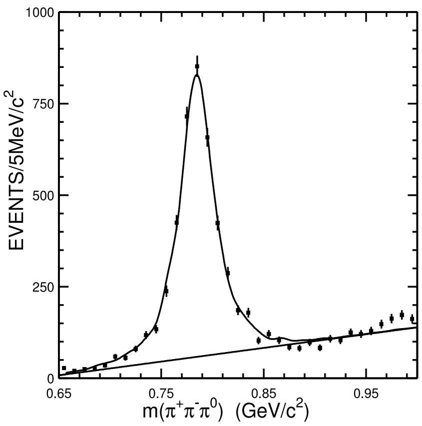

FIG. 4: The $m_{\pi^+\pi^-\pi^0}$ distribution for $J/\psi \to \omega\eta$ candidate events. The curves are the results of the fit described in the text.

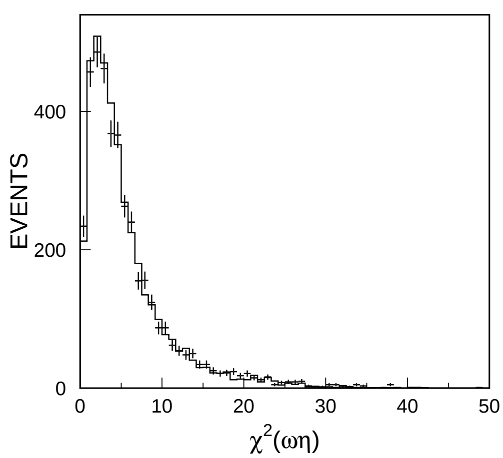

FIG. 5: The χ^2 distributions for the 4C fit to the $J/\psi \to \pi^+\pi^-\gamma\gamma\gamma\gamma$ hypothesis for $J/\psi \to \omega\eta$ candidate events. The crosses are data; the full histograms are the sum of MC simulation of $J/\psi \to \omega\eta$ and non-η background determined from η sidebands, as well as from $J/\psi \to \omega\eta(\eta \to \pi^0\pi^0\pi^0)$ and $J/\psi \to \omega\pi^0\pi^0$.

B. $J/\psi \to \omega\gamma\pi^+\pi^-$

For $J/\psi \to \omega\eta$, $\eta \to \gamma\pi^+\pi^-$, events with four well-reconstructed charged tracks and at least three isolated photons are required. A 4C-fit is performed to the $J/\psi \to \pi^+\pi^-\pi^+\pi^-\gamma\gamma\gamma$ hypothesis, and $\chi^2 < 20$ is required. There are 12 possible ways to combine the charged pions and gammas in forming the ω and η or η'.

1. $J/\psi \to \omega\eta$

Figure 6 shows the $\gamma\pi^+\pi^-$ invariant mass recoiling against the ω mass region, defined by $|m_{\pi^+\pi^-\pi^0} - 0.782| < 0.04$ GeV/c^2. A clear η signal is observed. The enhancement on the left side of the η in Figure 6 comes from $J/\psi \to \omega\eta$ ($\eta \to \pi^+\pi^-\pi^0$) with one photon missing. This interpretation as well as the asymmetric shape are confirmed by MC simulation.

The $\gamma\pi^+\pi^-$ mass distribution is then fitted by this enhancement with the shape determined from MC simulation, a Breit-Wigner to describe the η signal, and a first order polynomial background. The fit, shown in Figure 6, yields 284 ± 24 η candidate events. The contribution of the enhancement is consistent with the branching ratio for $J/\psi \to \omega\eta$ ($\eta \to \pi^+\pi^-\pi^0$). Fitting the $\gamma\pi^+\pi^-$ mass distribution of events recoiling against the ω sideband region (0.85 $< m_{\pi^+\pi^-\pi^0} <$ 1.0 GeV/c^2) and normalizing, 17 ± 6 non-ω background events are estimated and are subtracted. The detection efficiency obtained from MC simulation is 4.59%, and the corresponding branching fraction is

$$B(J/\psi \to \omega\eta) = (24.47 \pm 2.07) \times 10^{-4},$$

where the error is statistical.

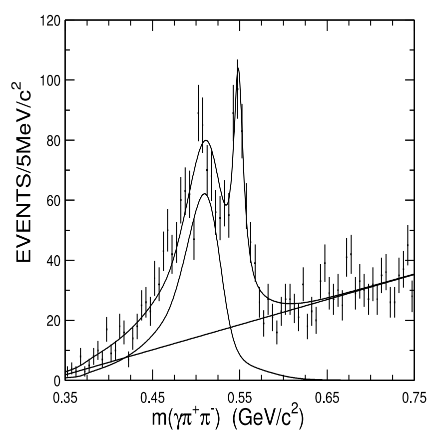

FIG. 6: Distribution of $m_{\gamma\pi^+\pi^-}$ for $J/\psi \to \omega\pi^+\pi^-\gamma$ candidate events. The crosses are data, and the curves are the results of the fit described in the text.

2. $J/\psi \to \omega\eta'$

After requiring $|m_{\pi^+\pi^-\pi^0} - 0.782| < 0.04$ GeV/c^2 using one pair of charged pions and the other pair of charged pions to be in the ρ mass region ($0.45 < m_{\pi^+\pi^-} < 0.92$ GeV/c^2), the distribution of $\gamma\pi^+\pi^-$ invariant mass recoiling against the ω mass region is shown in Figure 7, where a clear η' peak is seen. A

fit with the η' shape determined from MC simulation and a first order polynomial gives 197±27 η' candidate events. Fitting the $\gamma\pi^+\pi^-$ invariant mass distribution of events recoiling from the ω sideband region ($0.9 < m_{\pi^+\pi^-\pi^0} < 1.0$ GeV/c^2) and normalizing, yields 44 ± 11 non-η' background events, which are subtracted. The detection efficiency obtained from MC simulation is 4.24%, and the branching fraction is

$$B(J/\psi \to \omega\eta') = (2.41 \pm 0.33) \times 10^{-4},$$

where the error is statistical.

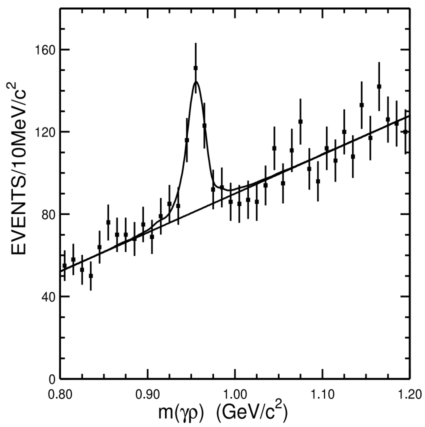

FIG. 7: Distribution of $m_{\gamma\pi^+\pi^-}$ for $J/\psi \to \omega\rho\gamma$ candidate events; the curves are the result of the fit described in the text.

C. $J/\psi \to \omega\pi^+\pi^-\gamma\gamma$

For $\eta \to \pi^+\pi^-\pi^0$ and $\eta' \to \pi^+\pi^-\eta$, events with four well reconstructed charged tracks and at least three isolated photons are selected. If there are four or more isolated photons, 4C kinematic fits to the $\pi^+\pi^-\pi^+\pi^-\gamma\gamma\gamma\gamma$ hypothesis are made. If there are only three isolated photons, a 1C kinematic fit with a missing photon is made, and the fit result is used to determine the momentum and energy of the missing photon. Because there are four pions and four photons, there are 24 possible ways to combine the charged pions and gammas in forming the ω and η or η'.

1. $J/\psi \to \omega\eta$

Figures 8 and 9 show the $m_{\gamma_1\gamma_2}$ and $m_{\gamma_3\gamma_4}$ distributions after the above selection and the additional requirements $|m_{\pi^+\pi^-\gamma_1\gamma_2} - m_\omega| < 0.04$ GeV/c^2 and $|m_{\pi^+\pi^-\gamma_3\gamma_4} - m_\eta| < 0.04$ GeV/c^2. Clear π^0 signals are observed, and the data and MC agree well.

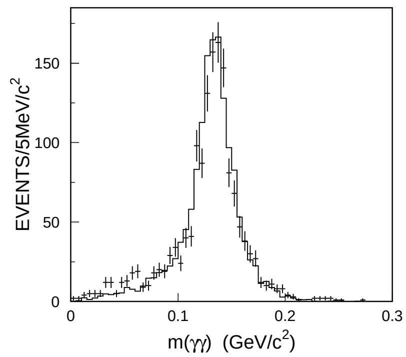

FIG. 8: The $m_{\gamma_1\gamma_2}$ invariant mass distribution for events satisfying $|m_{\pi^+\pi^-\gamma_1\gamma_2} - m_\omega| < 0.04$ GeV/c^2 and $|m_{\pi^+\pi^-\gamma_3\gamma_4} - m_\eta| < 0.04$ GeV/c^2 . The crosses are data and the histogram Monte Carlo simulation.

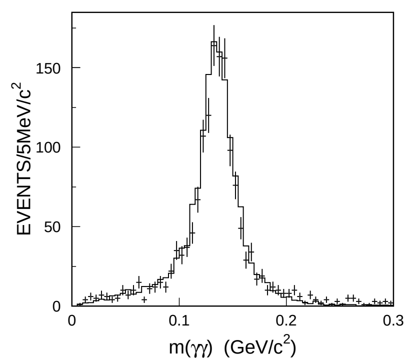

FIG. 9: The $m_{\gamma_3\gamma_4}$ invariant mass distribution for events satisfying $|m_{\pi^+\pi^-\gamma_1\gamma_2} - m_\omega| < 0.04$ GeV/c^2 and $|m_{\pi^+\pi^-\gamma_3\gamma_4} - m_\eta| < 0.04$ GeV/c^2. The crosses are data and the histogram Monte Carlo simulation.

The 4C and 1C χ^2 distributions for the fit to the $J/\psi \to \pi^+\pi^-\pi^+\pi^-\gamma\gamma\gamma\gamma$ hypothesis with the requirements that $m_{\gamma_1\gamma_2}$ and $m_{\gamma_3\gamma_4}$ are consistent with the mass of the π^0, ($|m_{\gamma\gamma} - 0.135| < 0.04$ GeV/c^2), and $m_{\pi^+\pi^-\pi^0}$ is in the η mass region ($|m_{\pi^+\pi^-\pi^0} - 0.547| < 0.04$ GeV/c^2), are shown in Fig. 10. The ratio of the numbers of events in the two plots for data is consistent with that from MC simulation. After the requirements $\chi^2 < 20$ for the 4C case and $\chi^2 < 5$ for the 1C case, the $m_{\pi^+\pi^-\pi^0}$ invariant mass spectrum recoiling against the η mass region ($|m_{\pi^+\pi^-\pi^0} - 0.547| < 0.04$ GeV/c^2), shown in Figure 11, is obtained. The ω shape obtained from MC simulation plus a second order polynomial are used to fit the $m_{\pi^+\pi^-\pi^0}$ mass distribution. A total of 1249±43 ω candidate events is obtained in the fit. The background determined using the η sideband region ($0.65 < m_{\pi^+\pi^-\pi^0} < 0.80$

GeV/c^2) is only 0 ± 2 events and thus can be ignored. Using the detection efficiency of 4.45%, the branching fraction of $J/\psi \to \omega\eta$ is

$$B(J/\psi \to \omega\eta) = (24.74 \pm 0.84) \times 10^{-4},$$

where the error is statistical.

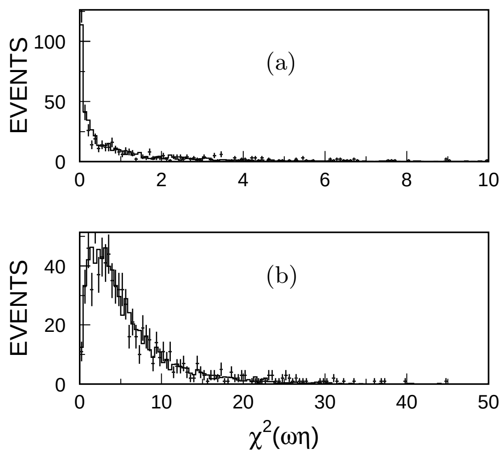

FIG. 10: The χ^2 distributions for the (a) 1C and (b) 4C fits to the $J/\psi \to \pi^+\pi^-\pi^+\pi^-\gamma\gamma\gamma\gamma$ hypothesis for $J/\psi \to \omega\eta, \eta \to \pi^+\pi^-\pi^0$ candidate events. The crosses are data, and the full histogram is the sum of the MC simulation of the signal channel and non-η background.

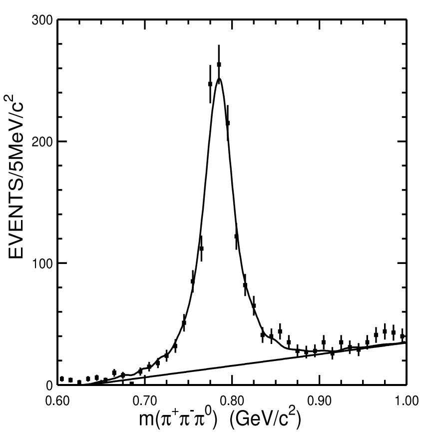

FIG. 11: The $m_{\pi^+\pi^-\pi^0}$ distribution for $J/\psi \to \omega\eta$, $\eta \to \pi^+\pi^-\pi^0$ candidate events. The curves are the results of the fit described in the text.

2. $J/\psi \to \omega\eta'$

After requiring two photons in the π^0 mass region and other two photons in the η mass region, *i.e.*, $|m_{\gamma_1\gamma_2} - 0.135| < 0.04$ GeV/c^2 and $|m_{\gamma_3\gamma_4} - 0.547| < 0.04$ GeV/c^2, as well as $\chi^2 < 15$ (5) for the 4C (1C) kinematic fit, the $\pi^+\pi^-\pi^0$ mass recoiling against the η' mass region ($|m_{\pi^+\pi^-\eta} - 0.958| < 0.04$ GeV/c^2), shows a clear ω peak, as seen in Figure 12. The fit of $m_{\pi^+\pi^-\pi^0}$ yields 65 ± 15 $\omega\eta'$ events. No events (0 ± 1) are observed in the distribution of events recoiling against the η' sidebands (1.10 GeV/c^2 $< m_{\pi^+\pi^-\eta} <$ 1.15 GeV/c^2) and are therefore ignored. Other backgrounds are also negligible. With the detection efficiency for this channel being 3.56%, we obtain

$$B(J/\psi \to \omega\eta') = (2.06 \pm 0.48) \times 10^{-4},$$

where the error is statistical.

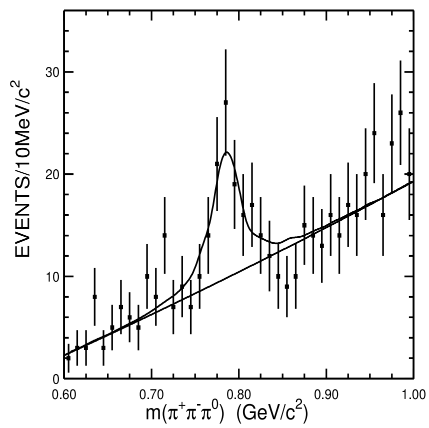

FIG. 12: The $m_{\pi^+\pi^-\pi^0}$ distribution for $J/\psi \to \omega\eta'$, $\eta' \to \pi^+\pi^-\eta$ candidate events. The curves are the result of the fit described in the text.

D. Systematic Errors

In this analysis, the systematic errors on the branching fractions mainly come from the following sources:

1. MDC tracking and kinematic fit

In order to study the systematic errors from the MDC tracking and kinematic fit, clean samples, such as $J/\psi \to \rho\pi$, $\Lambda\bar{\Lambda}$, $p\bar{p}$, K^*K, and $\psi(2S) \to \pi\pi J/\psi(J/\psi \to \mu^+\mu^-)$, are chosen, and many distributions from data, including the wire efficiency and resolution of charged tracks, are compared with those from MC simulations, using two different treatments of the wire resolution simulation. It is found that in most cases, the data distributions lie between the two MC simulations with the different treatments of the wire resolution. The simulation which agrees better with data is taken as the official MC simulation, and

the difference between the two simulations is taken as the systematic error for the tracking.

2. Particle Identification

In Refs. [6] and [9], the particle identification efficiency of pions is analyzed in detail. Here, only one charged track is required to be identified as a pion, and the systematic error from particle identification is less than 1% and is negligible.

3. Photon detection efficiency

The photon detection efficiency is studied using $J/\psi \to \rho^0\pi^0$ in Ref. [6]. The results indicate that the systematic error is less than 2% for each photon. There are slight differences in the π^0, η, and ω mass resolutions between MC and data. The effect of these differences on the branching ratios are very small and are ignored.

4. Uncertainty of background

The background uncertainties come from the uncertainties associated with the estimation of the sideband backgrounds, the continuum events, and the events from other background channels, as well as the uncertainties of the background shape, different fit ranges, *etc*. Therefore, the statistical errors in the estimated background events, the largest difference in changing the background shape and the difference of changing the fit range are taken as the systematic errors from the background uncertainty.

5. Intermediate decay branching fractions

The branching fractions of $\omega \to \pi^+\pi^-\pi^0$ and the pseudoscalar decays are taken from the PDG [7]. The errors of these branching fractions are systematic errors in our measurements and are listed in Table I.

The above systematic errors together with the error due to the uncertainty in the number of J/ψ events are all listed in Table I. The total systematic error is determined by adding all terms in quadrature.

IV. RESULTS

Table II lists the branching fractions of J/ψ decaying into $\omega\pi^0$, $\omega\eta$, and $\omega\eta'$. The average value is the weighted mean of the results from the different decay modes after taking out the common systematic errors, and the PDG value is the world average taken from Ref. [7]. The results are higher than those in the PDG as are our measurements of $J/\psi \to \pi^+\pi^-\pi^0$ [6] and $J/\psi \to \phi P(\pi^0, \eta, \eta')$ [8]. It emphasizes the importance of measuring the other decay modes of $J/\psi \to VP$, such as $J/\psi \to \rho\eta$, $\rho\eta'$, and K^*K based on the BESII $5.8 \times 10^7 J/\psi$ events.

Acknowledgments

The BES collaboration thanks the staff of BEPC and computing center for their hard efforts. This work is supported in part by the National Natural Science Foundation of China under contracts Nos. 10491300, 10225524, 10225525, 10425523, the Chinese Academy of Sciences under contract No. KJ 95T-03, the 100 Talents Program of CAS under Contract Nos. U-11, U-24, U-25, and the Knowledge Innovation Project of CAS under Contract Nos. U-602, U-34 (IHEP), the National Natural Science Foundation of China under Contract No. 10225522 (Tsinghua University), and the Department of Energy under Contract No.DE-FG02-04ER41291 (U Hawaii).

[1] H. E. Haber, J. Perrier, Phys. Rev. D **32**, 2961 (1985).
[2] R. M. Baltrusaitis *et al.*, Phys. Rev. D **32**, 2883 (1985).
[3] D. Coffman *et al.*, Phys. Rev. D **38**, 2695 (1988).
[4] J. Jousset *et al.*, Phys. Rev. D **41**, 1389 (1990).
[5] J. Z. Bai *et al.*, Nucl. Instrum. Methods A **458**, 627 (2001).
[6] J.Z.Bai et al., Phys. Rev. D70, 012005 (2004).
[7] S. Eidelman *et al.* (Particle Data Group), Phys. Lett. B **592**, 1 (2004), and references therein.
[8] M. Ablikim *et al.*, Phys. Rev. D **71**, 032003 (2005).
[9] M. Ablikim *et al.*, Nucl. Instr. and Meth. **A552**, 344 (2005).
[10] The angular distribution is described by $\frac{d^3\sigma}{d\cos\theta_V d\cos\theta_1 d\phi_1} = \sin^2\theta_1[1+\cos^2\theta_V + \sin^2\theta_V\cos(2\phi_1)]$ where θ_V is the angle between the vector meson and the positron direction. θ_1 and ϕ_1 describe the decay products of the vector meson in its helicity frame.

[11] S. S. Fang *et al.*, High Energy Phys. Nucl. Phys. **27**, 277 (2003) (in Chinese).

[12] R.M. Baltrusaitis et al., Phsy. Rev. D32, 566 (1985).

TABLE I: Systematic error sources and their contributions.

$J/\psi \to$	$\omega\pi^0$	$\omega\eta$			$\omega\eta'$	
Final state	$\pi^+\pi^-\gamma\gamma\gamma\gamma$	$\pi^+\pi^-\gamma\gamma\gamma\gamma$	$\pi^+\pi^-\pi^+\pi^-\gamma\gamma\gamma$	$\pi^+\pi^-\pi^+\pi^-\gamma\gamma\gamma\gamma$	$\pi^+\pi^-\pi^+\pi^-\gamma\gamma\gamma$	$\pi^+\pi^-\pi^+\pi^-\gamma\gamma\gamma\gamma$
Error sources	Relative Error (%)					
Wire resolution	6.9	9.1	11.6	11.3	13.3	10.3
Particle ID	<1	<1	<1	<1	<1	<1
Photon efficiency	$\sim$8	$\sim$ 8	$\sim$ 6	$\sim$ 8	$\sim$ 6	$\sim$ 8
Back. uncertainty	3.3	1.0	2.42	1.0	6.6	9.7
Intermediate decays	0.79	1.05	2.48	1.95	3.48	3.48
Total J/ψ events	4.72	4.72	4.72	4.72	4.72	4.72
Total systematic error	12.1	13.1	14.3	14.8	17.1	17.3

TABLE II: Branching fractions of $J/\psi \to \omega\pi^0$, $\omega\eta$, and $\omega\eta'$.

$J/\psi \to$	Final states	Branching Fraction ($\times 10^{-4}$)
$\omega\pi^0$	$\pi^+\pi^-\gamma\gamma\gamma\gamma$	5.38±0.12±0.65
	PDG	4.2 ± 0.6
$\omega\eta$	$\pi^+\pi^-\gamma\gamma\gamma\gamma$	22.86±0.43±2.99
	$\pi^+\pi^-\pi^+\pi^-\gamma\gamma\gamma$	24.47±2.07±3.50
	$\pi^+\pi^-\pi^+\pi^-\gamma\gamma\gamma\gamma$	24.74±0.85±3.66
	Average	23.52±2.73
	PDG	15.8±1.6
$\omega\eta'$	$\pi^+\pi^-\pi^+\pi^-\gamma\gamma\gamma$	2.41±0.33±0.41
	$\pi^+\pi^-\pi^+\pi^-\gamma\gamma\gamma\gamma$	2.06±0.48±0.36
	Average	2.26±0.43
	PDG	1.67±0.25